*Article*

# Structural Classification, Discharge Statistics, and Recession Analysis from the Springs of the Gran Sasso (Italy) Carbonate Aquifer; Comparison with Selected Analogues Worldwide

Giacomo Medici [1,*], Valeria Lorenzi [1] , Chiara Sbarbati [2] , Mauro Manetta [1] and Marco Petitta [1]

1   Dipartimento di Scienze della Terra, Universita' di Roma 'La Sapienza', Piazzale Aldo Moro 5, 00185 Roma, Italy; valeria.lorenzi@uniroma1.it (V.L.); manettamauro@gmail.com (M.M.); marco.petitta@uniroma1.it (M.P.)
2   Dipartimento di Scienze Biologiche ed Ecologiche, Universita' della Tuscia, 01100 Viterbo, Italy; chiara.sbarbati@unitus.it
*   Correspondence: giacomo.medici@uniroma1.it

**Abstract:** The relative importance of karst conduits and fractures in driving groundwater flow affects the discharge of springs and the long-term availability of water resources. Applying statistics to the hydrographs of the discharge and studying the recessions provide information on the degree of reliability and variability of the springs and, therefore, the flow regime within the saturated part of the carbonate aquifers. This approach was applied to six springs at the Gran Sasso aquifer in Central Italy. These springs were divided into three structural geological groups that determined the position of the permeability thresholds. The type of tectonic structures and the pattern of the permeability thresholds allow a correlation with the computed statistics. The studied springs were associated with the presence of thrusts, overturned drag folds, and a normal fault. The computed statistics describe a general scenario of reliability and steadiness for the springs. The Flow Duration Curves for the springs show limited groundwater flow through the conduits through a comparison with analogues in Slovakia. Joints and bedding plane fractures dominate the groundwater flow, fitting both the relative steadiness of the discharges and the pattern of the Flow Duration Curves. The recessions are also characterized by more gentle slopes with respect to nearby areas fitting a conceptual model of dominant fracture flow. This mathematical scenario depicts groundwater resources, which have limited exposure to episodes of summer droughts. The proposed approach is a holistic combination of structural geology and hydrologic elements and can be successfully exported to other tectonized carbonate areas for the sustainable management of groundwater resources worldwide.

**Keywords:** carbonate aquifers; groundwater sustainability; fractures; karst; discharge statistics; spring recessions

## 1. Introduction

Fractured aquifers of carbonate sedimentary origin, which are subjected to different degrees of karstification, underlie a land surface covering approximately 15% of the globe and supply about 25% of the world's population with potable water (Figure 1a) [1]. Hence, groundwater flow occurs through conduits and bedding planes, joints and fault-related fracture corridors rather than via pores in lithified carbonate rocks [2–6]. The relative importance of conduits and fractures in driving the groundwater flow affects the discharge rates at spring outlets and, therefore, the availability of natural water resources during the hydrological year in karst environments. Applying robust statistics to the hydrographs of the discharge and studying the recession provide information on the reliability, degree of variability, and also the flow regime within the saturated part of the fractured and karst aquifers [7–12]. Due to the economic and civil importance of the karst water resources, a statistical study of the discharge regime started back in the 1920s with the introduction

of the first statistical parameters [13]. After this first input, other parameters have been introduced to classify the discharge, e.g., [14–16]. Some of these attempts were relatively recent, and are summarized in the methodological paper [9].

A statistical study of the discharge time series and the analysis of the recessions are also useful to manage natural groundwater resources. A mathematical definition of a hydrologic scenario that is expected to vary over the next years is fundamental, due to the expected effects of climate change that affects the infiltration and the aquifer recharge dynamics [17–23]. Therefore, the proposed topic has received renewed interest in the last fifteen years in the karst hydrogeological literature, being an attempt to analyse exposure to water scarcity that can be exacerbated in the near future [24–29]. The study of the recession of the springs provides information on the risk of water scarcity; highly karstified systems are more exposed to such a risk due to a combination of either rapidly decreasing discharge rates or water availability during the spring and summer times [30].

The research presented also combines an analysis of the discharge time series and recession with a careful study of the structural geology settings of the karst springs. A study of the structural geology combined with statistics of discharge time series and recession represents the novelty of this work. The presented mathematical parameters and curves were compared only with topography and aquifer recharge dynamics by previous authors [13–16]. Here, we discuss new mathematical results with structural geology, topography, and aquifer recharge dynamics to contrast previous studies.

This attention aims to provide additional information on the groundwater flow to the springs that can guide the interpretation of the discharge time series. The selected area for the combination of a study of the structural setting, discharge, and recession of the springs is the Gran Sasso Massif in Central Italy (Figure 1b,c) [31]. The site was selected in the framework of the Karst Aquifer Resources Availability and Quality in the Mediterranean Area (KARMA) project that was funded by the European Union [32,33].

The peculiarity of this project site is related to the elevated levels of spring withdrawals for drinking water use and its location within the Gran Sasso and Laga Mountains National Park, reflecting the need to supply water to the human population without compromising the environment and ecosystems. As a result of these needs, the most recent hydrogeological literature focuses on the dynamics of the recharge of the aquifer in the Gran Sasso Range. Here, the infiltration rates of the aquifer system were recently constrained using precipitation, temperature, and snow depth data, and the different proportions of rainfall and snowmelt on the aquifer recharge were discussed in detail [34]. The high infiltration rates were found at the Campo Imperatore plain due to the direct input of snow to the aquifer recharge. Groundwater stable isotopes were used to assess the influence of snowpack on the recharge dynamics of some carbonate massifs of Central Italy, including the Gran Sasso [35,36]. By contrast, the proposed research offers a focus on the discharge points of the selected carbonate aquifer system. The research therefore advances the conceptualization of the aquifer to achieve a virtuous management of the groundwater resources at the Gran Sasso and Laga Mountains National Park.

The Gran Sasso ridge is dominated by dolostone and limestone of Meso-Cenozoic age, and large paleokarst features such as dolines with diameters of tens of meters, along with the absence of large caves [37–39]. The study site is located in the proximity of the Marche region. Here, recent studies from [40,41] applied the same model to the recessions, thus allowing for a comparison (Figure 1b).

Overall, our goal is to characterize both conceptually and mathematically the discharge regime of the springs at Gran Sasso to verify the exposure of the natural groundwater resources to potential stresses, such as the reduction of the infiltration rates or the increase of withdrawals. The specific objectives are as follows: (i) to classify the springs from a structural point of view in order to unravel the dynamics of groundwater flow, (ii) to statistically characterize the discharge time series, (iii) to highlight a link between the structural setting, and the computed statistics, and (iv) to study the spring recession by using the classical Maillet model [42].
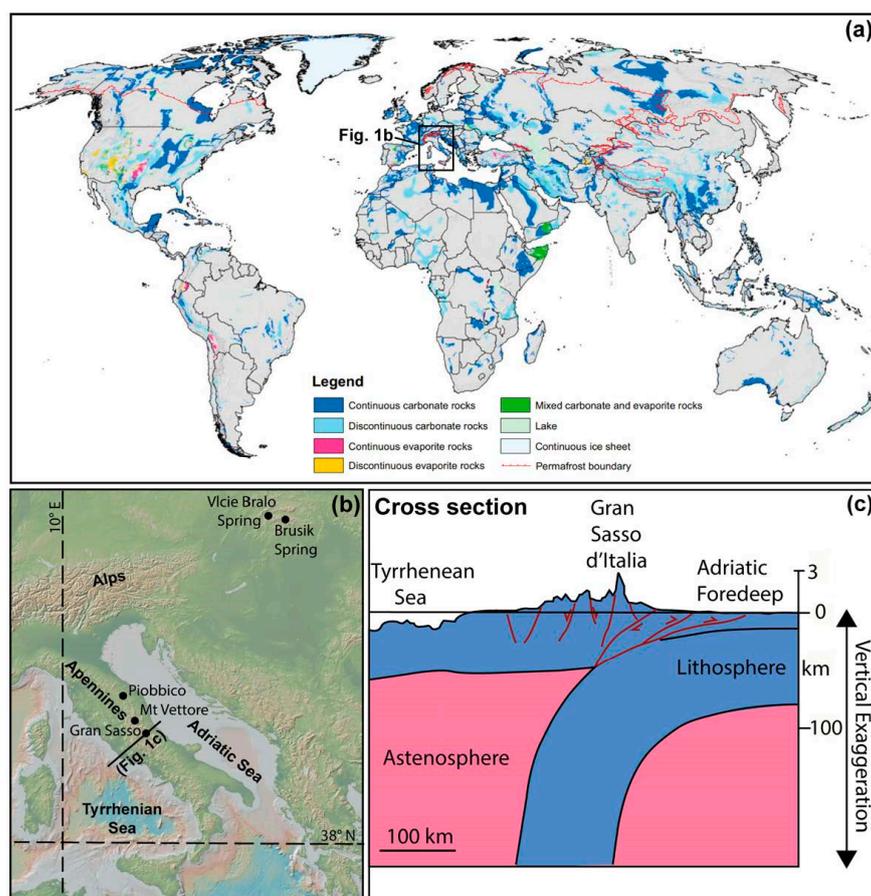
**Figure 1.** Study area. (**a**) worldwide map of karst aquifers of carbonate, evaporate and ice sheet origin (Goldscheider et al., 2020) [1]; (**b**) map of Italy [31] with black dots on the field site and studied analogues of Mount Vettore, Piobbico and the two Slovakian springs; (**c**) geodynamic cross-section [31] with the Gran Sasso in evidence.

## 2. Study Area

### 2.1. Geological Setting

The Gran Sasso Range is part of the Apennine fold and thrust belt formed at the expense of the western continental margin of the Adria plate (Figure 1b,c). The Apennine Mountains are an exhumed earlier stage of the accretionary prism, now dismounted by extensional faults of the Quaternary age [43]. Thrusts and normal faults, and fractures related to the folding highly influence the groundwater flow at the study site [44,45] and are therefore described in this section. The Gran Sasso Massif is located on the eastern side of the Apennines (Figure 1b) that has been exhumed by thrusts later than the part of the belt adjacent to the Tyrrhenian Sea. Hence, this study site has been at least partially preserved by exposure to weathering and kastification, compared to the western part of the Italian peninsula [37,46]. A stratigraphy ranging from Late Triassic to Late Miocene and Quaternary is in exposure at the study site is depicted on the left side panel in Figure 2. Following the Triassic lagoon and tidal flat lithofacies of the Dolomia Principale Formation, the area was characterized by shallow water deposits of carbonate platform during the Earliest Jurassic time with the deposition of the Calcare Massiccio Formation. Later, during the late Early Jurassic time, the platform was displaced by faulting and marine ingression occurred. The carbonate platform drowned and pelagic and turbiditic calcareous sediments were deposited in a large sedimentary basin (Corniola and Verde Ammonitico formations, Figure 2). Notably, such deposits are mechanically much more layered than the massive dolostone and limestone underneath (Figure 2). Other common lithotypes are characterized by marls, calcarenites of bioclastic origin, and mudstones [31]. A variety

of marly limestones characterized the later Middle–Late Jurassic and Cretaceous times and are mechanically highly layered (Corno Piccolo, Cherty Detrital Limestone, Maiolica, Cefalone, Scaglia Bianca, Monte Corvo, and Fote Gelata formations, Figure 2). The middle Miocene movements were interpreted in [47], as related to a tectonically deformed foreland, which started during the Oligocene, as suggested by the opening of Paleogene dykes of neptunian origin, and the presence of marls, which occurred in the studied succession since the Oligocene time (Venacquaro Formation).

The Miocene succession begins with cherty and glauconitic calcarenites, followed by the calcarenites and pelagic marls of the Cerrogna Marl Formation. The youngest preorogenic formation of the region is the Orbulina Marl Formation (Tortonian—early Messinian), consisting of 10–15 m thick bioturbated hemipelagic marls, abundant in planktonic foraminifera. The overlying Laga Flysch Formation (Figure 2) is a 0.5–2.5 km thick succession of turbidite sandstone and shale pinching out against the frontal structure of the Gran Sasso d'Italia [48,49].

## 2.2. Hydrogeological Setting

The Gran Sasso Massif hosts a groundwater table with an average hydraulic gradient ranging from 5 to 20% [44]. The aquifer has a total discharge of 18–25 $m^3/s$ from its springs, including a motorway tunnel drainage tapped for potable water use on both sides [50–53]. Aquifer recharges calculated in [34] for the last twenty years by three different methods show similar and reliable outputs; yearly mean infiltration ranges from 558 (Thornthwaite method) to 606 mm/y (Turc method), with an incidence lower than 10% (Aplis method yields 594 mm/y). The Campo Imperatore plain appears to be the main recharge area, where a thick snowpack is yearly deposited during the late autumn and winter times. Indeed, the snowmelt contribution to the recharge is important, reaching 98 mm/y [34,35].
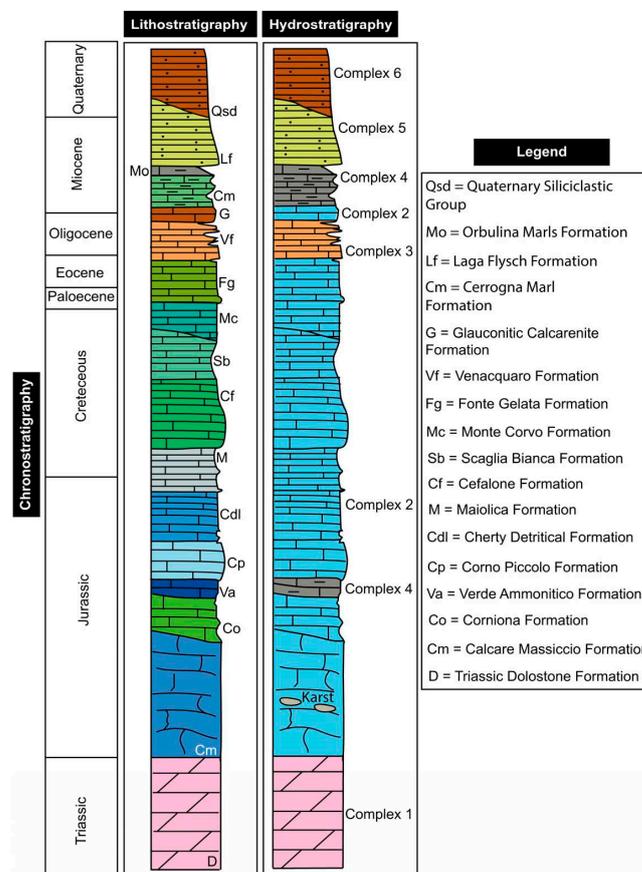


**Figure 2.** Lithostartigraphic [31], and hydrostratigraphic [54] columns of the study site.

The complex stratigraphy (see left side panel in Figure 2) can be hydrogeologically summarized by organizing the lithostratigraphy into six complexes (see right side panel in Figure 2) that have been proposed in the hydrogeological map published by [54]. The dolostones of the Triassic age (C1, Figure 3a) are characterized by lower hydraulic conductivities and storativities from pumping tests and, therefore, characterize a single hydrostratigraphic complex, which are less affected by processes of groundwater dissolution [54]. The permeable limestones of the Mesozoic and Cenozoic age characterizes the Hydrostratigraphic Complex 2 (Figure 3b,c and Figure 4). Notably, this aquifer complex is characterized by a paloeokarst horizon that occurs in the lower part of the Calcare Massiccio Formation as depicted in the hydrostratigraphic column in Figure 2 [55].
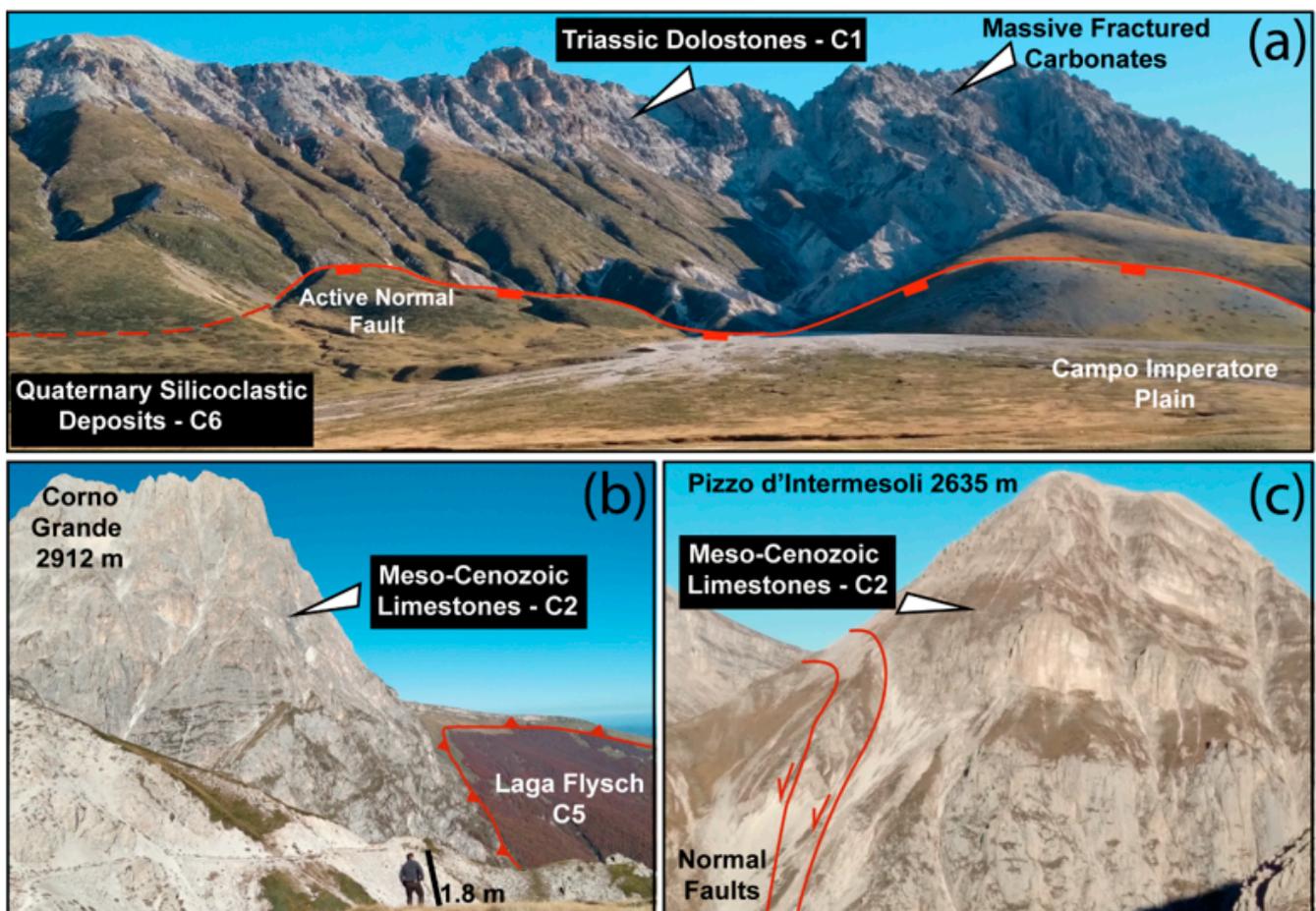


**Figure 3.** Hydrostratigraphic complexes in outcrop in the Gran Sasso area. (**a**) active normal faults with Triassic Dolostones (C1), and Quaternary Siliciclastic Deposits (C6) in the footwall and hanging wall, respectively; (**b**) Panoramic view of the Meso-Cenozoic Limestones (C2), the principal thrust, and the Laga Flysch (C5) deposits; (**c**) Normal faults displacing the Meso-Cenozoic Limestones (C2) at Pizzo d'Intermesoli.

The Oligocene marly limestones of the Venacquaro Formation characterize Complex 3, which behaves as an aquifer across the study site (Figure 2). The relatively low permeability of Verde Ammonitico of the Jurassic age, the Cerrogna, and the Orbilina Marls of the Miocene age are all calcareous marls, corresponding to the local aquitards, Complex 4. The overlying Laga Flysch Formation, Complex 5 (Figures 2 and 3b), is highly heterogeneous and is characterized by turbiditic sandstones and shales that behave as aquitard or even aquiclude [54]. The youngest hydrogeological complex is named Quaternary Siliciclastic Deposits (C6) and is characterized by sands and clays related to alluvialconoids, lacustrine, and fluvial sedimentary architectural elements. These sedimentary deposits

show permeabilities from low to high; overall, the permeability is lower for C6 than the principal aquifer C2 [54]. C6 is divided in two complexes of the Quaternary age and is of siliciclastic sedimentary in origin in the 1:150,000 Hydrogeological Map of the Gran Sasso area [54]. C6 has been assumed a single complex in this research due to the fact that the quaternary deposits do not play a role with respect to the six selected springs. Overall, the carbonate complexes C1, C2, and C3 behave as aquifers, and their contacts with the terrigenous aquitard/aquiclude units C4, C5, and C6 are characterized by the presence of springs [51,54]. The latter units (C4, C5, and C6), as all aquitards, have the capacity to increase the resident time of more than one order of magnitude and attenuate the capacity of the contaminants to reach the portions of the aquifer which are located stratigraphically and structurally at a lower level [54].
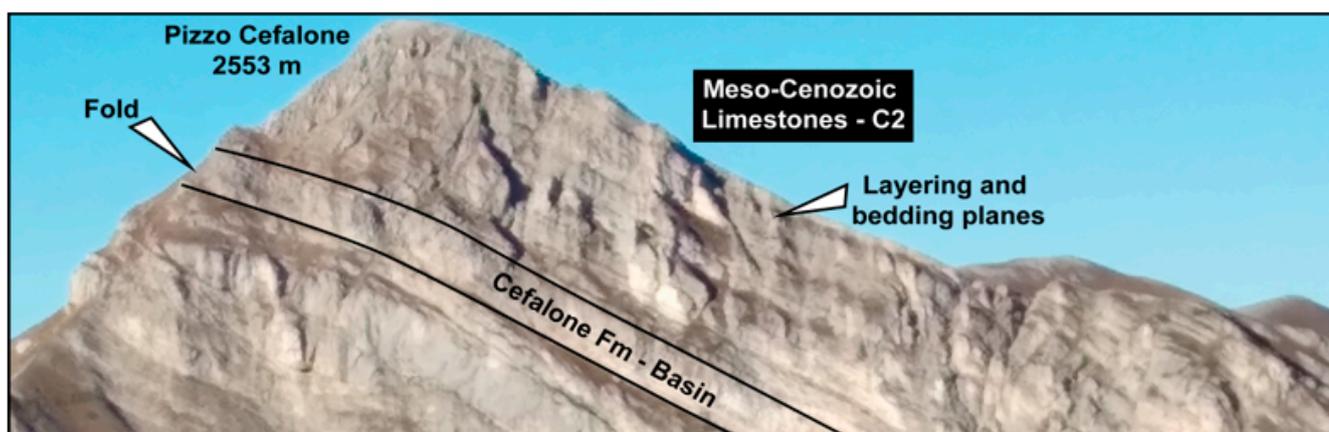


**Figure 4.** Focus on the complex of the Meso-Cenozoic Limestones (C2) showing a fold in the basin deposits of the Pizzo Cefalone Formation part of the Meso-Cenozoic Limestones (C2).

Hydrochemistry for groundwater quality purposes was studied in all the springs of the Gran Sasso National Park including those studied in this research that shows a focus on the physical hydrogeology [51,54]. Groundwater was classified by analyzing the major ions using piper plots. The water samples were classified as a Ca–Mg–HCO$_3$ type, which is typical of a carbonate aquifer characterized by either limestones or dolostones [50]. Saturation indexes show positive and negative values for calcite and dolomite, respectively. Oxygen, hydrogen, carbon, and radon isotopes were also studied over the years to unravel the areas and dynamics of aquifer recharge [35,36,50]. Overall, the fractured dolostones and limestones of the Gran Sasso and Laga Mountains National Park host huge and high-quality groundwater resources according to [50,52].

### 3. Methods

Six springs located in the northern part of the studied ridge have been studied in this research: Vacelliera Alta (VA), Vacelliera Bassa (VB), South Motorway Tunnel (MT), Vitella d'Oro (VO), Mortaio d'Angri (MA), and Chiarino (CH) (Figure 5). These springs have been analysed to unravel the structural settings that create barriers to the groundwater flow across the Gran Sasso Massif (Figure 1b,c; Table 1). Daily records of the discharge were analysed to classify these springs according to the magnitude of the discharge and the degree of reliability and variability. The recession curves were also studied to unravel the flow regime crossing the information with a structural characterization and the statistics of the discharge.
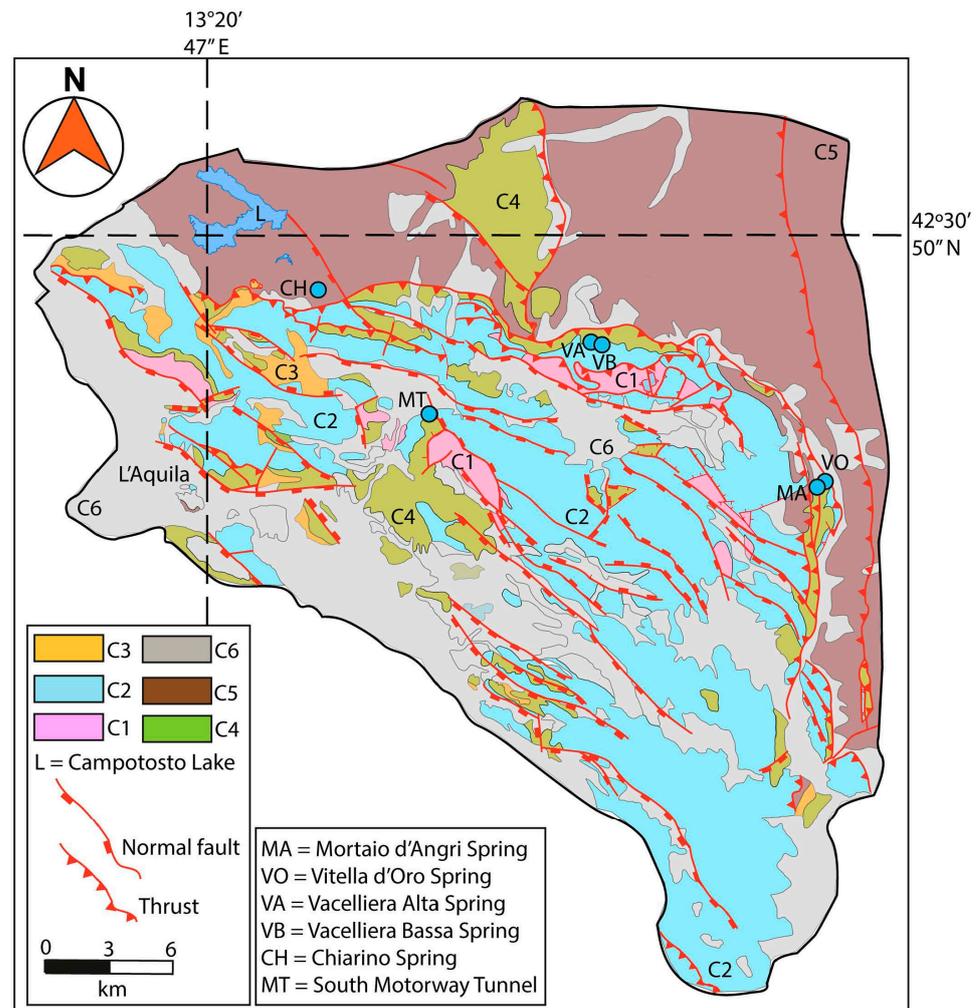
**Figure 5.** Simplified Version of the Hydrogeological Map of the Gran Sasso Area [54] with location of the six springs in Table 1, and the six hydrostratigraphic complexes: Triassic dolsotones (C1), Meso-cenzoic limestones (C2), Early Cenozoic Marls (e.g., Vernaquero Formation) (C3), Verde Ammonitico, Cerrogna and Orbulina Marls formations (C4), Laga Flysch Formation (C5), and Quaternary Siliciclastic deposits (C6).

### 3.1. Structural Classification

The selected six springs were plotted on the 1:150,000 Hydrogeological Map (Figure 5) of the Gran Sasso Massif [54]. The six springs are all mapped in the northern part of the study site. Here, the thickness and the areal extension of the Quaternary Siliciclastic Deposits (C6) are lower than in the southern part; this portion of the Gran Sasso site is, therefore, excellent for studying the impact of the tectonic lines and the lithologies of bedrock on the groundwater flow.

The position of thrusts and normal faults are extracted from the 1:50,000 Geological Map of the Gran Sasso d'Italia 349 Sheet, Geological Map of Italy [56]. Given the location of the six springs plotted on the ArcGIS version of the 1:150,000 Hydrogeological Map of the Gran Sasso Massif [54], the springs were classified using the scheme proposed by [57]. This scheme was recently used by a variety of authors to define the structural setting, e.g., [58,59], and define the springs based on the position of the low permeability threshold that can be located either above or below the aquifer unit.

The position of the aquitard, aquiclude and aquifer units depends on the presence of folds, thrusts, and extensional faults at the study site. Faults can divide the same aquifer unit, and the fault zone can represent a permeability threshold. In the latter case, the

traditional scheme (Table 1) of the hydrogeology of faults has been used [60], and the spring is related to a fault barrier that has been intercepted by an infrastructure.

**Table 1.** Hydrostratigraphic complexes, permeability thresholds, topography, and type of geological contact that play a role on the presence of the six springs studied at the Gran Sasso. The classification of the permeability threshold is based on two hydrogeological schemes [57,60].

| Spring | Topographic Elevation (mASL) | Aquifer; Aquitard | Classification Permeability Threshold | Geological Contact Aquifer /Aquitard | Spring Goups |
|---|---|---|---|---|---|
| Vacelliera Alta (VA) | 1018 | Mesozoic limestones (C2); Orbulina Marls Formation (C4) | Underneath [57] | Stratigraphic | Group 1 |
| Vacelliera Bassa (VB) | 990 | Mesozoic limestones (C2); Orbulina Marls Formation (C4) | Underneath [57] | Stratigraphic | Group 1 |
| Vitella d'Oro (VO) | 650 | Mesozoic limestones (C2); Orbulina Marls Formation (C4) | Underneath [57] | Thrust | Group 2 |
| Mortaio d'Angri (MA) | 690 | Mesozoic limestones (C2); Orbulina Marls Formation (C4) | Underneath [57] | Thrust | Group 2 |
| Chiarino (CH) | 1330 | Mesozoic limestones (C2); Laga Formation (C5) | Underneath [57] | Thrust | Group 2 |
| South Motorway Tunnel (MT) | 982 | Mesozoic limestones (C2); Mesozoic limestones (C2) | Fault core [60] | Normal fault | Group 3 |

### 3.2. Statistics

All six springs have been classified according to the discharge magnitude, degree of variability based on arithmetic average, and the maximum and minimum of the discharge by applying rigorous statistics (classes shown in Tables 2 and 3) to the available dataset (time span analysed of the daily time series in Table 4). Springs in karst environments are classified based on the average annual discharge in terms of magnitude [13]. The simplest measure of discharge Reliability and Variability reported in this research is the ratio ($Q_{max}/Q_{min}$) of maximal and minimum discharge defined in groundwater hydrology as the $I_v$ Index [9]. Based on the $I_v$, six and four categories of Reliability and Stability, respectively, have been proposed and discussed (Table 2). Of note, the degrees of Reliability and Stability are defined by the same Index ($I_v$), and they are directly proportional. Indeed, a spring which is reliable provides a similar amount of water during the hydrological year and, therefore, it must also be relatively stable. To reduce the effect of extreme outliers on the spring's classification that occurs on measuring the Reliability and Variability degrees with $I_v$, other mathematical parameters of discharge time series were computed (Spring Variability Index, Spring Variability Coefficient, and Spring Variation Coefficient Parameter). Ref. [13] proposed a measure of variability V expressed by Equation (1).

$$V = \frac{(Q_{max} - Q_{min})}{\varnothing} \times 100\% \tag{1}$$

where V represents the Spring Variability Index expressed in %, $Q_{max}$ and $Q_{min}$ are defined above, and $\varnothing$ is the arithmetical mean of spring discharge values. The discharge is considered highly constant for V lower than 25%, moderately constant for values ranging from 25% and 100%, and variable for values higher than 100% as summarized in Table 2 [9,13].

**Table 2.** Reliability and Stability classes for karst springs based on $I_v$ [9].

| Degree of Spring Reliability | $I_v$ |
|---|---|
| Excellent | 1.0–3.0 |
| Very Good | 3.1–5.0 |
| Good | 5.1–10.0 |
| Modest | 10.1–20.0 |
| Bad | 20.1–100.0 |
| Very Bad | >100.0 |
| Ephimeral Spring | ∞ |
| **Degree of Spring's Discharge Stability** | **$I_v$** |
| Highly Stable | 1.0–2.0 |
| Moderately Stable | 2.1–10.0 |
| Unstable | 10.1–30.0 |
| Totally Unstable | >30.0 |

**Table 3.** Classes [9] of spring discharge variability (V, SVC and SVCP), and stability (SVC).

| Spring Variability Index | V (%) |
|---|---|
| Highly constant | <25 |
| Moderately constant | 25–100 |
| Variable | >100 |
| **Degree of Spring Variability** | **SVC** |
| Steady | 1.0–2.5 |
| Well balanced | 2.6–5.0 |
| Balanced | 5.1–7.5 |
| Unbalanced | 7.6–10.0 |
| Highly unsteady | >10.0 |
| Ephemeral | ∞ |
| **Degree of Spring Discharge Stability** | **SVC** |
| Very Stable | 1.0–3.0 |
| Stable | 3.1–10.0 |
| Unstable | 10.1–20.0 |
| VeryUnstable | 20.1–100.0 |
| Extremely Unstable | >100.0 |
| **Degree of Spring Variability** | **SVCP** |
| Low | 0–49 |
| Moderate | 50–99 |
| High | 100–199 |
| Very High | >200 |

The spring variability has also been studied using the Spring Variation Coefficient Parameter (SVCP) proposed by [15] as the ratio between the standard deviation (σ) of the spring discharge and arithmetic mean (∅). Spring discharges are classified in four SVCP categories, as summarized in Table 3. The Spring Variability Coefficient (SVC) is

another statistical parameter computed to analyse the available time series and is the ratio ($Q_{10}/Q_{90}$) of the discharges Exceedance.

**Table 4.** Summary of the statistical parameters studied for the six selected springs in the Gran Sasso area.

| Spring | Arithmetic Average, Q (L/s) | Standard Deviation, Q (L/s) | SVCP | V (%) | SVC | $I_v$ | Years |
|---|---|---|---|---|---|---|---|
| Vacelliera Alta (VA) | 57.3 | 19.6 | 0.34 | 149 | 0.44 | 5.65 | 2017–2022 |
| Vacelliera Bassa (VB) | 139.9 | 37.4 | 0.27 | 99 | 0.50 | 3.09 | 2017–2022 |
| South Motorway Tunnel (MT) | 467.2 | 37.9 | 0.10 | 24 | 0.64 | 1.33 | 2016–2018 |
| Vitella d'Oro (VO) | 304.6 | 49.9 | 0.16 | 66 | 0.62 | 1.96 | 2015–2021 |
| Mortaio d'Angri (MA) | 251.9 | 68.8 | 0.27 | 128 | 0.48 | 3.21 | 2017–2022 |
| Chiarino (CH) | 112.2 | 34.4 | 0.31 | 84.7 | 0.47 | 2.58 | 2005–2008 |

$Q_{10}$ represents a discharge value that is exceeded 10% of the time and $Q_{90}$ represents discharge that is exceeded 90% of the time. SVC categories are five and are also summarized in Table 3. $Q_{10}$ and $Q_{90}$ are extrapolated by the Flow Duration Curves (FDC) that consist of plotting the discharge (Q) and the Exceedance on the *x* and *y* axes, respectively. Note that, SVCP and SVC describe the degree of variability of the discharge at the spring outlet, but SVC is mathematically related to the FDC that is also part of the presented computational efforts. The Exceedance value can be extrapolated by the percentiles and is defined as a residue between 1 and the Exceedance in a decimal format (0.7 for 30 % Exceedance or 0.95 for 5 % Exceedance) [9]. The Exceedance curve from the six springs studied in the Gran Sasso area has been compared to the one from a fractured dolostone aquifer (Vlcie Bralo Spring in the Muranska Planina Plateau; Figure 1b) and a karstified limestone (Brusik Spring in the Velka Fatra Mountains; Figure 1b) in Slovakia as proposed by [9].

*3.3. Spring Recession Analysis*

The recession was extrapolated from the six springs, showing a yearly decrease in the discharge values using daily data. The formula from [42] describes the recession by comparing a spring to an analogical model of a water reservoir emptying through a plug with pores. The formula is described by Equation (2) which has been used to fit the recession curves for all the six springs.

$$Q_t = Q_0 e^{-\alpha t} \tag{2}$$

where $Q_0$ (L·s$^{-1}$) is the initial discharge before the onset of the recession, $Q_t$ (L·s$^{-1}$) is the discharge at time t (also studied to determine $I_v$, V, SVCP, and SVC), and $\alpha$ is the recession coefficient expressed in reciprocal time units (day$^{-1}$). Values of the maximum, minimum, and arithmetic average for $\alpha$ were computed, accounting for the individual recession curve at each spring. The combined regression for $\alpha$ was computed fitting together all the available data points at each spring to enable the comparison with the recession analysis from the nearby Marche region in Arquata del Tronto/Mount Vettore [41] and Piobbico [40] (Figure 1a,b). The years that were considered for the six springs, which exclusively analyse daily data, are shown in Table 4. A larger time (10 to 25 years) span is available with monthly, bi-monthly, and yearly data for the six selected springs. The yearly low frequency and discontinuous datasets agree with the presented one in terms of the yearly arithmetic averages of the discharge ensuring that the selected dataset is reliable at a larger time scale.

**4. Results**

*4.1. Structural Classification*

Two of the six springs at the study site, VA and VB are related to a stratigraphic contact (Table 1). The Miocene Cerrogna and Orbulina Marls (C4) are located below the Meso-

Cenozoic Limestones (C2) by an overturned fold in the central and northern sectors of the study site. In these sectors of the study area, the complex of the Marly Limestones (C3) can be absent due to reduced accommodation space in the sedimentary basin (Figure 5). In correspondence with the VA and VB springs, the stratigraphic succession is reversed due to the presence of a drag fold in the proximity of a thrust and the permeability threshold is located below the contact (Group 1 of springs in Table 1). The VO, MA, and CH springs (Group 2 in Table 1) are characterized by a permeability threshold located beneath the thrust. The relatively low permeability aquiclude is represented by the Cerrogna and Orbulina Marls (C4) for the VO and MA springs (Figure 5). Here, a thrust fault creates contact between C2 and C5; the tip of the thrust is buried ~20 m below a sedimentary cover of conglomerates of the Messinian age according to the Gran Sasso d'Italia 349 Sheet of the Geological Map of Italy.

The relatively low permeability barrier for the groundwater flow is characterized by the Laga Flysch deposits (C5) that are located beneath the Meso-Cenozoic limestones (C2) according to the hydrogeological map in Figure 5 for the CH Spring. The latter spring is located 300 m north respect to the principal thrust fault; the tectonic contact is responsible for the emergency of the groundwater, but the spring is topographically located at a lower level. Ref. [57] includes this exception and the permeability threshold can be classified as located below the tectonic contact (Table 1). The MT Spring is related to the drainage of a highway tunnel 10 km in length that cuts the Gran Sasso Massif. The fault zone intersects the same complex of the Meso-Cenozoic limestones (C2), and the permeability threshold is represented by the fault core. The scheme of the hydrogeology of faults is therefore used to classify this specific spring located at the western edge of the tunnel of the motorway (Group 3 in Table 1).

### 4.2. Statistics

A statistical analysis of the spring discharge has been applied using a variety of parameters. The magnitude of the spring discharge is defined according to the arithmetic average reported in Table 4, distinguishing the eight classes (1st to 8th from a higher to lower degree of magnitude) [13]. The MA, VB, MT, VO, and CH are in the 2nd class with average discharges ranging from 112.2 to 467.2 L/s. The arithmetic average of the discharge is 57.3 L/s for VA, which is characterized by the lowest magnitude value and is therefore classified in the 3rd class (Table 4).

The discharge can be classified either in terms of Reliability or Stability using the $I_v$ value. MT, VO, and CH are Excellent in terms of Reliability by crossing the classes in Table 2 and the values in Table 4. According to the same tables, VB and MA are Very Good and VA is Good. In terms of Stability, VO and MT are Highly Stable and CH, VA, MA, and VB are Moderately Stable (Tables 2 and 4).

The degree of variability can also be studied using V, which is defined by Equation (2). The MT is Constant, being characterized by V% < 25%. VB, VO, and CH are intermediate between Constant and Variable, showing V values ranging from 25% and 100%. VA and MA are characterized by a Variable discharge (V > 100%; Tables 2 and 4). Overall, MT appears the most reliable, stable, and steady spring from the combination of $I_v$ and V values summarized in Table 4. The topography does not play the key role in determining the degree of reliability, stability, and steadiness for the MT Spring. This MT spring is classified as third in terms of the topographic elevation at the study site (Table 1).

The same combination of statistical parameters highlights VA and MA as relatively unstable and variable springs (Table 4). VA is topographically located above and in the proximity of VB and MA above and in the proximity of VO (Figure 5).

All six springs are characterized by a low degree of variability according to the SVCP at the study site by crossing the values in Table 4 with the classes in Table 2. The same six springs are Very Stable and Steady, according to the SVC ($Q_{10}/Q_{90}$) values of the discharges (Exceedance of the discharge), in terms of Variability and Stability, respectively (see values in Table 4 and classes in Table 3). Notably, SVCP and SVC show an overall scenario of

steadiness for all six springs. A slightly lower degree of variability is shown by $I_v$ and V. This discrepancy arises from the presence of the maximum ($Q_{max}$) and minimum ($Q_{min}$) discharges in the $I_v$ and V formula as explained above in the methodology section. SVCP is characterized by the highest (0.34) and lowest (0.10) values for VA and MT, respectively. The ratio between the minimum and maximum SVCP values is 0.29 according to the values summarized in Table 4. The SVCP values for MA and VB are also high with respect to the MT (Table 4).

SVC values are similar among the six springs studied and they range from 0.44 to 0.64 (Table 4). The ratio between the minimum and maximum SVC is indeed 0.69 (see values in Table 4). SVC can be extrapolated by the FDC in Figure 6, which contains other information on the spring discharges of the Gran Sasso aquifer system. The FDC of the MT spring is flat, typical of carbonate aquifers, subject to reduced rock dissolution by groundwater flow. In fact, the FDC for MT matches the flat curve representative of a fractured dolostone of the Vlcie Bralo Spring (Figure 6). VA, VB, and MA show FDC curves that are steeper with respect to both the South Motorway Tunnel and Vlcie Bralo springs (Figure 6). The scenario of the FDC curves finds a fit with the computed $I_v$ and V values. In fact, MT represents an end member in terms of Reliability and Stability of the discharge according to the low values of $I_v$ and V (Table 4). The FDCs can also be related to the topography. The CH spring is classified as Structural Group 2 and is characterized by the highest topographic elevation and is the flattest according to the FDCs (Table 1; Figure 6). VB is topographically lower and steeper than VA, according to the FDC. Both the springs (VB and VA) are located in the same valley, and classified in the same structural group (Group 1; Table 1). By contrast, MA is topographically higher, and steeper than VO, according to the FDC fitting a direct correlation between steepness and higher topography (Figure 6). Both the springs are located in the same valley and classified in Structural Group 2 (Table 1). MT represents the only spring classified in Group 3 and is topographically located at the intermediate level in the study site (Table 1). This spring represents an end member in terms of Reliability and Stability as shown in Table 4.
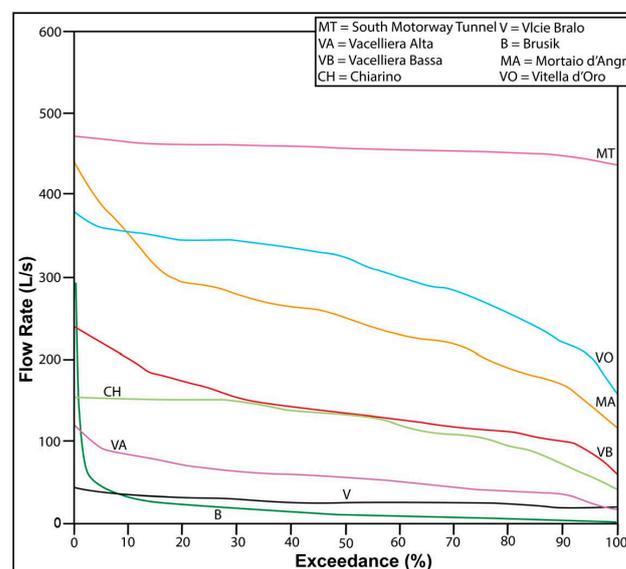


**Figure 6.** Flow Duration Curves for the Vacelliera Alta, Chiarino, Vacelliera Bassa, Mortaio d'Angri, Vitella d'Oro, and South Motorway Tunnel at the study sites, and the Vlcie Bralo and Brusik springs in Slovakia.

VA and MA are characterized by the highest values of $I_v$ and V, and the discharges are relatively unstable. VA is also characterized by the highest SVCP value, that although so high, shows a very low degree of Variability according to Table 3. The FDC curve of MA is the steepest for Exceedance values from 0% to 10% fitting high values of $I_v$ and V. This FDC

is also the closest to one of the highly kastified Brusik Springs in the Velka Fatra Mountains (Slovakia) among the six selected springs (Figure 6). However, the FDC curves computed for VA, VB, MT, VO, MA, and CH do not fit the analogue of a highly karstified limestone proposed by [9] that shows a very steep slope for Exceedance values ranging from 0% to 10% (Figure 6).

### 4.3. Spring Recession Analysis

The recession curves (Figure 7) were extrapolated from the available dataset with the specific years that are shown in Table 5. The springs are characterized by a gentle decrease in the discharges during the late spring–summer–early autumn period. This time of recession shows averages of 92 days (CH Spring), 145 days (VA Spring), 146 days (VO Spring), 148 days (VB Spring), and 180 days (MA, and MT springs) (Figure 7). The gently decreasing discharge is highlighted by the low values of the recession coefficients ($\alpha$) from both the arithmetic means and the combined recession (Table 5) that are computed by fitting the curves using Equation (2). The combined recession analysis also shows relatively low $\alpha$ values (0.001–0.010 day$^{-1}$; Figure 7; Table 5) by comparing the results with those from [40,41]. These authors applied the same model to the groups of springs located between 35 and 100 km (see locations of Mount Vettore and Piobbico in Figure 1b) north respect to the Gran Sasso, finding $\alpha$ values ranging from 0.006 to 0.013 day$^{-1}$. $R^2$ values range from 0.21 to 0.83, which are lower than the karst springs of the Marche region ($R^2$ = 0.92–0.97). VB is characterized by a particularly low $R^2$ (0.21) value by analysing all six years of discharge monitoring; this statistical parameter rises to 0.91 and 0.92 by grouping the years 2017, 2018, and 2019 and 2020, 2021, and 2022, respectively (Figure 7). Notably, the lowest $R^2$ value (0.53) from the combined regression analysis was computed for the MT spring, which also shows particularly low values of $I_v$, SVCP, and V (Table 5) and the flattest FDC (Figure 6) among the six selected springs.
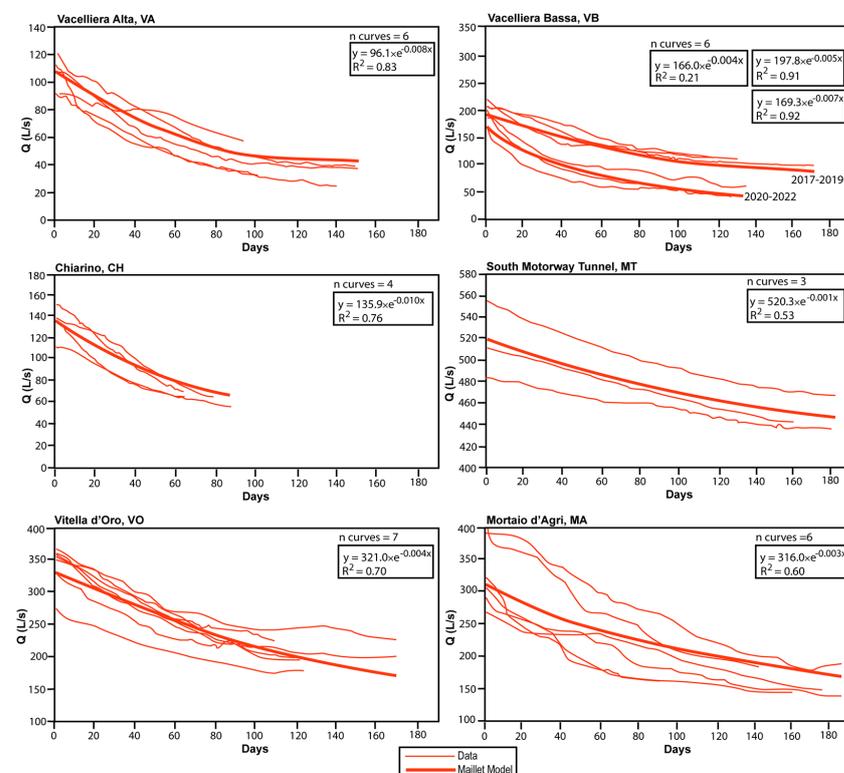


**Figure 7.** Recessions for six springs at the study site with results from the application of Maillet formula [42].

**Table 5.** Summary of $\alpha$ values (minimum, maximum, standard deviation, and combined regression) generated from the application of the Maillet model [42] for six selected springs at the study site.

| Spirngs | Minimum–Maximum | Average | Standard Deviation, σ | Combined Regression |
|---|---|---|---|---|
| Vacelliera Alta (VA) | 0.005–0.012 | 0.009 | 0.0021 | 0.008 |
| Vacelliera Bassa (VB) | 0.004–0.013 | 0.007 | 0.0032 | 0.004 |
| South Motorway Tunnel (MT) | 0.0006–0.001 | 0.001 | 0.0002 | 0.001 |
| Vitella d'Oro (VO) | 0.0003–0.006 | 0.004 | 0.0009 | 0.004 |
| Mortaio d'Angri (MA) | 0.003–0.008 | 0.005 | 0.0019 | 0.003 |
| Chiarino (CH) | 0.009–0.013 | 0.011 | 0.0015 | 0.010 |

## 5. Discussion

### 5.1. Structural Setting of the Springs, Topography and Groundwater Flow

Normal faults (Figure 3a,c), thrusts (Figure 3b), and folds (Figure 4) play a key role in driving the groundwater flow at the field site, as well as in other areas dominated by carbonate rocks, as shown in the conceptual models in Figure 8a–c. In this research, we stress the structural geology as a factor that plays a role in the discharge regime of the six springs that are recharged from the same area (the Campo Imperatore plain, shown in Figure 5) according to the most recent $\delta^{18}O$ isotope analyses [36]. The source of recharge can, therefore, be discarded as useful in interpreting the computed hydrologic parameters. However, the structural geology settings and the topography can vary among the six springs and, therefore, need to be discussed to interpret the dynamics of spring discharge in the karst environment [7,8]. Three springs (MA, VO, and CH) are aligned along the easternmost and principal thrust of the Gran Sasso Range (Figure 3b). The permeability threshold is placed below the thrust (Figure 8a) and the aquitard is either represented by the Orbulina Marls (C4) or the Laga Flysch (C5) formations. The presence of an overturned drag fold (Figure 8b) places the permeability threshold below the contact aquifer/aquitard for the VA and VB springs with the aquitard represented by the Miocene Marls (C4). All the springs that are either aligned with or located in the proximity of a thrust show a similar FDC pattern (Figure 6) and a good degree of Reliability and Stability according to the statistics summarized in Table 4.

Springs VA, VB, CH, and MA show relatively steeper FDCs, relatively high values of $I_v$ and V, and high values of SVCP (the highest is for Vacelliera Alta as shown in Table 4). The latter statistical parameter (SVCP) can be related to the structural setting; the VA and VB are located where the beds are sub-vertical due to the intense compressional tectonics that affected the study site during the Cenozoic era [31,47,49]. VO and MA are located where multiple splays of the thrust sheet are mapped and the area is relatively more karstified with elevated topographic gradients, which are up to 0.92 [51,61]. Notably, MA is characterized by an FDC pattern that is the steepest among the studied springs but far from the steepness of the karst limestone of the Brusik Spring in Slovakia (Figures 1b and 6). The steepness of MA can be explained by the fact that it is located at a higher altitude compared to VO in the same valley (Figure 5; Table 1) and, therefore, is characterized by a more unstable flow regime. However, MA is not the highest spring on the scale in the northern sector of the Gran Sasso (Figure 4; Table 1).
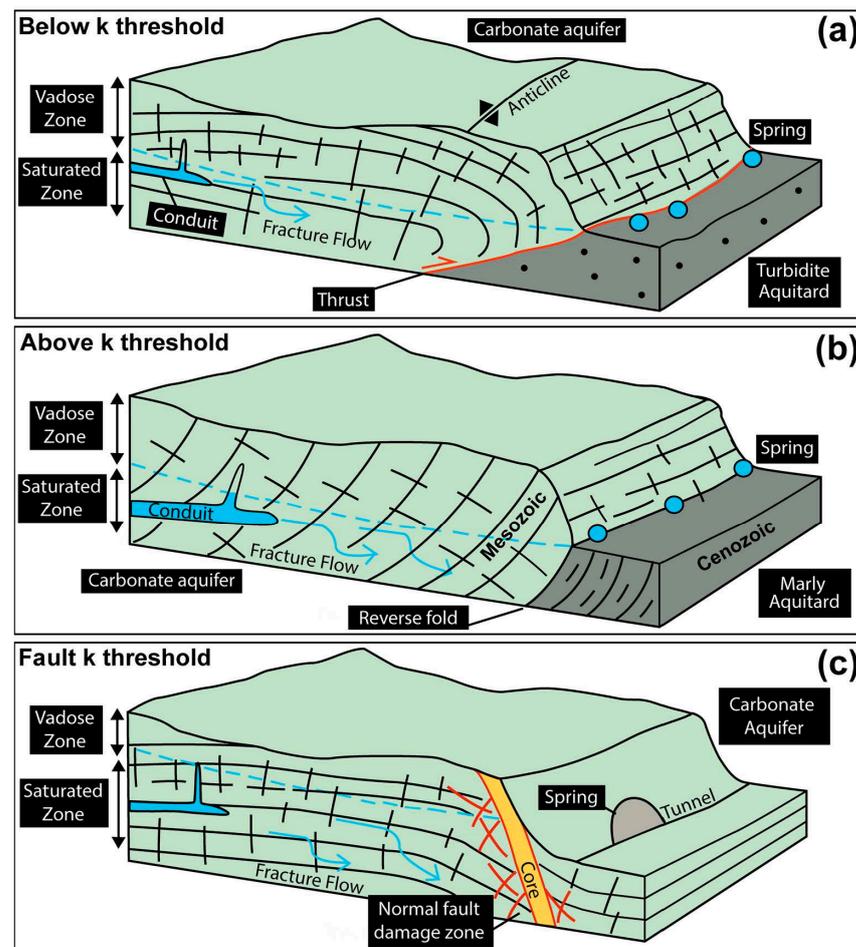
**Figure 8.** Conceptual scheme of the carbonate aquifer of the Gran Sasso area in different structural settings with detail on the permeability (k) threshold. (**a**) springs aligned along a thrust fault with permeability threshold underneath sensu [57], (**b**) springs related to drag fold with permeability threshold underneath sensu [57], (**c**) spring related to normal faulting and construction of a tunnel relative importance.

This general scenario of high reliability of the natural water resources of the Gran Sasso is also supported by the proposed structural classification. Indeed, a scenario of high reliability and steadiness of the springs over the hydraulic years has been tested in different tectonic settings and, hence, can be extended to the entire northern area of the Gran Sasso. Looking at the structural settings and the computed statistics in more detail, it can be noted that MT is characterized by a relatively flat Flow Duration Curve. Three statistical parameters (V, $I_v$, and SVCP) also show the highest degree of Reliability and Stability for the MT spring. This hydraulic pattern reflects a different structural geology setting. The latter spring is the only one that is related to an extensional fault (Figure 8c), which represents a permeability barrier that separates two blocks of the Meso-Cenozoic Limestones (C2). The water table was partially drained since the 1980s because of underground infrastructure development of the highway tunnels and underground laboratories of the National Institute of Nuclear Physics [44,51,52,62]. Groundwater drainage is captured by an infrastructure located under the highway tunnel and, therefore, the MT spring represents an artificial discharge point. The motorway tunnel intercepts an extensional fault zone characterized by a high transmissivity and storage coefficient [51]. In fact, the fault core and damage zone (Figure 8c) are capable of feeding a spring of 467.2 L/s average discharge, which makes the MT number one in terms of magnitude among the selected springs (Table 4). Overall, this spring (MT), located along a normal fault, is characterized by SVCP, V, and $I_v$ two to five

times lower when compared with either the springs in heavy folds in the proximity of a thrust (VA, and VB; Group 1) or springs (VO, MA, and CH; Group 2) with the emergence of water related to the thrust (Tables 1–3). This scenario depicts the control the structural geology has on the hydrological statistics that were not found by all the recent statistical studies on spring discharges, e.g., [7,10,12,26,40,41,63]. The structural style is not the only factor that plays a role in the computed statistics. Indeed, the topography can influence, to some extent, the degree of steadiness and reliability of the springs, as shown by the VO and MA springs. The springs, which are located higher topographically, can be relatively less stable and reliable.

*5.2. Insights for Groundwater Resources Management*

The carbonate aquifer of the Gran Sasso Massif is characterized by reliable and relatively stable spring discharges according to the statistical parameters ($I_v$, V, SVCP, and SVC; Table 4) computed in this proposed research. In addition to this scenario of steadiness and reliability, all the studied recessions are gentle in comparison to the slopes of the recessions found in the nearby carbonate areas of the Marche region [40,41,44]. The fractures play the key role in driving the groundwater flow to the springs as highlighted by the low coefficients of the combined recession (0.001–0.01 day$^{-1}$, 0.004 day$^{-1}$ for range and the median, respectively) and the difficulties of applying the Maillet model ($R^2 < 0.85$) across the entire study area. Issues with applying the Maillet model can be related to either bias in the dataset, due to multiple contributions to the spring discharges (e.g., overflow, flow from different systems in the subsurface), or the high contribution of the fractures driving the groundwater flow. The latter explanation is supported by the low $R^2$ (0.53) from the recession at the MT where a fractured fault damage zone has been intercepted [52]. Here, all the statistical parameters in Table 4, as well as the FDC pattern, show the dominance of fracture flow fitting low $R^2$. This relatively weak correlation suggests difficulties with applying a traditional methodology of karst hydrology (e.g., the Maillet formula for representation of the recession) to a system that is not highly karstified. As a consequence of the importance of fracture flow at the study site, Discrete Fracture Network models can be generated to simulate reactive contaminant transport at a relatively small scale (e.g., 10 km$^2$) [64]. Indeed, the transport and removal of contaminants in groundwater is a key issue in fractured sedimentary rocks in Central Italy as well as worldwide [65–68]. The Equivalent Porous Medium can be used at the regional scale (100–1000 km$^2$) to represent the flow through the fractures at the Gran Sasso. Discrete conduits can be inserted in the three-dimensional domain of a future regional model to represent karstified areas of reduced spatial extension (a few meters in diameter and tens of meters to a few kilometers in length) [69,70]. This implementation would refine the model output in terms of hydrological balance to achieve rigorous management of the groundwater resources at the study site.

The flow regime described above arises from reduced dissolution that is related to the combination of: (i) the presence of dolostones and dolomitized carbonate having a significant thickness, (ii) the relative abundance of marls, and (iii) the dominance of highly layered limestones (Figure 2). These three types of rocks are less prone to dissolution than massive limestones, thereby matching the principal role of fracture flow in the different tectonic settings found in this research [70].

This geological scenario fits the computational results. Fractures play a key role in driving groundwater flow based on three mathematical evidences. Firstly, the combined recession analysis shows relatively low $\alpha$ values (0.001–0.010 day$^{-1}$; Figure 7; Table 5) when compared with the results of [40,41] in other areas of the Apennines. Secondly, fitting the recessions using the traditional karst methodology represented by the Maillet formula is difficult as shown by the low coefficients of determination, $R^2$ (Figure 7). Thirdly, all the FDCs are much less steep at the study site than the one at the Brusik Spring in Slovakia, which is described in the literature as being representative of highly karstified limestones (Figure 6). This mathematical scenario finds an application in terms of groundwater resource management. Despite the carbonate origin of the studied aquifer, its springs are

less prone to rapid decreases in discharge and, hence, less exposed to summer droughts that can occur in karst environments [2,30,71]. According to the results of our study, the springs of the Gran Sasso appear to be able to withstand periods of water scarcities and can thus serve as an emergency water supply for nearby areas.

## 6. Conclusions

The relative importance of conduits and fractures in driving groundwater flow affects the discharge of springs and the availability of natural water resources in karst environments. Applying a statistical analysis to the hydrographs of the discharge and studying the recessions provide information on the degree of reliability and variability of the springs and, therefore, can elucidate the saturated part of carbonate aquifers. This approach has been applied to six springs in the Gran Sasso area in different tectonic scenarios. The results are summarized as follows and include a comparison with selected carbonate analogues:

1. The six selected springs were divided into three different structural geology settings that control the presence of permeability thresholds and the emergence of the groundwater. The studied springs were structurally associated with the presence of thrusts, drag folds, and a normal fault. Classifying the springs according to the tectonic setting contributes to a deeper knowledge of the groundwater resource, and also allows comparisons with the computed statistical parameters ($I_v$, V, and SVCP), and FDCs.

2. The statistics applied to six selected springs using several parameters ($I_v$, V, SVC, and SVCP) describe a general scenario of reliability and steadiness. The Flow Duration Curves, when compared with Slovakian analogues, show reduced flow through the karst conduits. Joints and bedding plane fractures play a key role in driving the groundwater flow at the study site, fitting both the relative steadiness of the springs and the pattern of the FDCs.

3. Structural geology and the completed statistics show a degree of correlation. Springs aligned along a major thrust with sub-vertical beds and multiple splays in the catchment area are relatively more karstified (e.g., MA Spring). Values of $I_v$, V, and SVCP are higher and the FDC steeper with respect to other settings. However, the MT spring, which is associated with a normal fault, is characterized by the fattest FDC. The statistical parameters also show the highest degree of Reliability and Stability for the spring (MT Spring) mapped along that fault and the southern edge of a tunnel. The extensional fault represents a permeability barrier that separates two blocks of fractured limestones.

4. When applied to the available daily time series, the Maillet formula shows recession curves that gently decrease in terms of flow rate. This pattern appears more evident when the curves from the Gran Sasso springs are compared with those of the nearby Marche region, which is characterized by an analogous stratigraphy. The springs of the Gran Sasso are characterized by lower $\alpha$ values, which fit a scenario of relative steadiness of the discharges and groundwater resources that are less exposed to episodes of summer drought.

Our findings that indicate a large degree of reliability of the groundwater resources were validated in different structural geology settings and, hence, can be extended to the entire area of the Gran Sasso. Our approach is holistic and it can be successfully exported to other tectonized carbonate areas to achieve sound management of groundwater resources worldwide.

## References

1.  Goldscheider, N.; Chen, Z.; Auler, A.S.; Bakalowicz, M.; Broda, S.; Drew, D.; Hartmann, J.; Jiang, G.; Moosdorf, N.; Stevanovic, Z.; et al. Global distribution of carbonate rocks and karst water resources. *Hydrogeol. J.* **2020**, *28*, 1661–1677. [CrossRef]
2.  Hartmann, A.; Goldscheider, N.; Wagener, T.; Lange, J.; Weiler, M. Karst water resources in a changing world: Review of hydrological modeling approaches. *Rev. Geophys.* **2014**, *52*, 218–242. [CrossRef]
3.  Maldaner, C.H.; Quinn, P.M.; Cherry, J.A.; Parker, B.L. Improving estimates of groundwater velocity in a fractured rock borehole using hydraulic and tracer dilution methods. *J. Contam. Hydrol.* **2018**, *214*, 75–86. [CrossRef]
4.  Agbotui, P.Y.; West, L.J.; Bottrell, S.H. Characterisation of fractured carbonate aquifers using ambient borehole dilution tests. *J. Hydrol.* **2020**, *589*, 125191. [CrossRef]
5.  Maldaner, C.H.; Munn, J.D.; Coleman, T.I.; Molson, J.W.; Parker, B.L. Groundwater flow quantification in fractured rock boreholes using active distributed temperature sensing under natural gradient conditions. *Water Resour. Resear.* **2021**, *55*, 3285–3306. [CrossRef]
6.  Worthington, S.R.; Jeannin, P.Y.; Alexander, E.C.; Davies, G.J.; Schindel, G.M. Contrasting definitions for the term 'karst aquifer'. *Hydrogeol. J.* **2017**, *25*, 1237–1240. [CrossRef]
7.  Fiorillo, F. Tank-reservoir drainage as a simulation of the recession limb of karst spring hydrographs. *Hydrogeol. J.* **2011**, *19*, 1009–1019. [CrossRef]
8.  Fiorillo, F. The recession of spring hydrographs, focused on karst aquifers. *Water Resour. Manag.* **2014**, *28*, 1781–1805. [CrossRef]
9.  Malík, P. Evaluating discharge regimes of karst aquifer. In *Karst Aquifers—Characterization and Engineering*; Stevanović, Z., Ed.; Springer: Berlin, Germany, 2015.
10. Posavec, K.; Giacopetti, M.; Materazzi, M.; Birk, S. Method and Excel VBA algorithm for modeling master recession curve using trigonometry approach. *Groundwater* **2017**, *55*, 891–898. [CrossRef]
11. Torresan, F.; Fabbri, P.; Piccinini, L.; Dalla Libera, N.; Pola, M.; Zampieri, D. Defining the hydrogeological behavior of karst springs through an integrated analysis: A case study in the Berici Mountains area (Vicenza, NE Italy). *Hydrogeol. J.* **2020**, *28*, 1229–1247. [CrossRef]
12. Malík, P.; Švasta, J.; Bajtoš, P.; Gregor, M. Discharge recession patterns of karstic springs as observed in Triassic carbonate aquifers of Slovakia. *Hydrogeol. J.* **2021**, *29*, 397–427. [CrossRef]
13. Meinzer, O.E. *The Occurrence of Ground Water in United States with a Discussion of Principles*; USGS Water-Supply Paper: Washington, DC, USA, 1923.
14. Netopil, R. The classification of water springs on the basis of the variability of yields. *Stud. Geogr.* **1971**, *22*, 145–150.
15. Flora, S.P. Hydrogeological Characterization and Discharge Variability of Springs in the Middle Verde River Watershed, Central Arizona. Master's Thesis, Northern Arizona University, Flagstaff, AZ, USA, 2004.
16. Kresic, N. *Hydrogeology and Groundwater Modeling*, 2nd ed.; CRC Press, Taylor and Francis: Boca Raton, FL, USA, 2007.
17. Ravbar, N.; Goldscheider, N. Comparative application of four methods of groundwater vulnerability mapping in a Slovene karst catchment. *Hydrogeol. J.* **2009**, *1*, 725–733. [CrossRef]
18. Allocca, V.; De Vita, P.; Manna, F.; Nimmo, J.R. Groundwater recharge assessment at local and episodic scale in a soil mantled perched karst aquifer in southern Italy. *J. Hydrol.* **2015**, *529*, 843–853. [CrossRef]
19. Ruggieri, G.; Allocca, V.; Borfecchia, F.; Cusano, D.; Marsiglia, P.; De Vita, P. Testing evapotranspiration estimates based on MODIS satellite data in the assessment of the groundwater recharge of karst aquifers in southern Italy. *Water* **2021**, *13*, 118. [CrossRef]
20. Doummar, J.; Kassem, A.H.; Gurdak, J.J. Impact of historic and future climate on spring recharge and discharge based on an integrated numerical modelling approach: Application on a snow-governed semi-arid karst catchment area. *J. Hydrol.* **2020**, *565*, 636–649. [CrossRef]

21. Kovačič, G.; Petrič, M.; Ravbar, N. Evaluation and quantification of the effects of climate and vegetation cover change on karst water sources: Case studies of two springs in south-western slovenia. *Water* **2020**, *12*, 3087. [CrossRef]

22. Sanz Pérez, E.; Fonolla, C.; Menéndez Pidal, I.; Rosas Rodriguez, P. Paleohydrogeology of the karstic system of fuentetoba spring (Soria, spain): An interdisciplinary approach. *Sustainability* **2021**, *13*, 7236. [CrossRef]

23. Medici, G.; Langman, J.B. Pathways and Estimate of Aquifer Recharge in a Flood Basalt Terrain; A Review from the South Fork Palouse River Basin (Columbia River Plateau, USA). *Sustainability* **2022**, *14*, 11349. [CrossRef]

24. Springer, A.E.; Stevens, L.E. Spheres of discharge of springs. *Hydrogeol. J.* **2009**, *17*, 83–93. [CrossRef]

25. Mudarra, M.; Andreo, B. Relative importance of the saturated and the unsaturated zones in the hydrogeological functioning of karst aquifers: The case of Alta Cadena (Southern Spain). *J. Hydrol.* **2011**, *397*, 263–280. [CrossRef]

26. Cinkus, G.; Mazzilli, N.; Jourde, H. Identification of relevant indicators for the assessment of karst systems hydrological functioning: Proposal of a new classification. *J. Hydrol.* **2021**, *603*, 127006. [CrossRef]

27. Portoghese, I.; Masciale, R.; Caputo, M.C.; De Carlo, L.; Malcangio, D. Combined Discharge and Thermo-Salinity Measurements for the Characterization of a Karst Spring System in Southern Italy. *Sustainability* **2020**, *12*, 3311. [CrossRef]

28. Sivelle, V.; Jourde, H.; Bittner, D.; Mazzilli, N.; Tramblay, Y. Assessment of the relative impacts of climate changes and anthropogenic forcing on spring discharge of a Mediterranean karst system. *J. Hydrol.* **2021**, *598*, 126396. [CrossRef]

29. Beckford, H.O.; Chang, C.; Ji, H. Determination of Paleoenvironmental Changes by Using $\delta13C$, 14C Dating and Rb/Sr Ratio in Critical Karst Area of Yunnan-Guizhou Plateau, Southwestern China. *Sustainability* **2023**, *15*, 6480. [CrossRef]

30. Leitner, S.; Dirnböck, T.; Kobler, J.; Zechmeister-Boltenstern, S. Legacy effects of drought on nitrate leaching in a temperate mixed forest on karst. *J. Environ. Manag.* **2020**, *262*, 110338. [CrossRef]

31. Cardello, G.L.; Doglioni, C. From mesozoic rifting to Apennine orogeny: The gran Sasso range (Italy). *Gondwana Res.* **2013**, *27*, 1307–1334. [CrossRef]

32. Goeppert, N.; Goldscheider, N.; Berkowitz, B. Experimental and modeling evidence of kilometer-scale anomalous tracer transport in an alpine karst aquifer. *Water Res.* **2020**, *178*, 115755. [CrossRef]

33. Xanke, J.; Liesch, T. Quantification and possible causes of declining groundwater resources in the Euro-Mediterranean region from 2003 to 2020. *Hydrogeol. J.* **2022**, *30*, 379–400. [CrossRef]

34. Lorenzi, V.; Sbarbati, C.; Banzato, F.; Lacchini, A.; Petitta, M. Recharge assessment of the Gran Sasso aquifer (Central Italy): Time-variable infiltration and influence of snow cover extension. *J. Hydrol. Reg. Stud.* **2022**, *41*, 101090. [CrossRef]

35. Petitta, M.; Banzato, F.; Lorenzi, V.; Matani, E.; Sbarbati, C. Determining recharge distribution in fractured carbonate aquifers in central Italy using environmental isotopes: Snowpack cover as an indicator for future availability of groundwater resources. *Hydrogeol. J.* **2022**, *30*, 1619–1636. [CrossRef]

36. Lorenzi, V.; Barberio, D.M.; Sbarbati, C.; Petitta, M. Groundwater recharge distribution due to snow cover in shortage conditions (2019-22) on the Gran Sasso carbonate aquifer (Central Italy). *Environ. Earth Sci.* **2023**, *82*, 206. [CrossRef]

37. Bisci, C.; Gentili, B.; Ciccacci, S.; Dramis, F.; Kotarba, A. The extent of Pleistocene glaciations in the western part of the Campo Imperatore (Gran Sasso Massif, Central Italy). *Landf. Anal.* **1999**, *2*, 37–43.

38. Tallini, M.; Gasbarri, D.; Ranalli, D.; Scozzafava, M. Investigating epikarst using low-frequency GPR: Example from the Gran Sasso range (Central Italy). *Bull. Eng. Geol. Environ.* **2006**, *65*, 435–443. [CrossRef]

39. Pecci, M.A.; D'Aquila, P.I. Geomorphological features and cartography of the Gran Sasso d'Italia massif between Corno Grande-Corno Piccolo and Pizzo Intermesoli. *Geogr. Fis. Din. Quat.* **2011**, *34*, 127–143.

40. Giacopetti, M.; Materazzi, M.; Pambianchi, G.; Posavec, K. Analysis of mountain springs discharge time series in the Tennacola stream catchment (central Apennine, Italy). *Environ. Earth Sci.* **2017**, *76*, 20. [CrossRef]

41. Valigi, D.; Fronzi, D.; Cambi, C.; Beddini, G.; Cardellini, C.; Checcucci, R.; Mastrorillo, L.; Mirabella, F.; Tazioli, A. Earthquake-induced spring discharge modifications: The Pescara di Arquata spring reaction to the August–October 2016 Central Italy earthquakes. *Water* **2020**, *12*, 767. [CrossRef]

42. Maillet, E. *Essais D'hydraulique Soutarraine et Fluviale*; Librarie Scientifique: Paris, France, 1905.

43. Carminati, E.; Doglioni, C. Alps vs. Apennines: The paradigm of a tectonically asymmetric. *Earth Earth Sci. Rev.* **2012**, *112*, 67–96. [CrossRef]

44. Amoruso, A.; Crescentini, L.; Petitta, M.; Rusi, S.; Tallini, M. Impact of the 6 April 2009 L'Aquila earthquake on groundwater flow in the Gran Sasso carbonate aquifer, Central Italy. *Hydrol. Process.* **2011**, *25*, 1754–1764. [CrossRef]

45. Amoruso, A.; Crescentini, L.; Petitta, M.; Tallini, M. Parsimonious recharge/discharge modeling in carbonate fractured aquifers: The groundwater flow in the Gran Sasso aquifer (Central Italy). *J. Hydrol.* **2013**, *476*, 136–146. [CrossRef]

46. Miccadei, E.; Piacentini, T.; Esposito, G. Geomorphosites and geotourism in the parks of the Abruzzo region (Central Italy). *Geoheritage* **2011**, *3*, 233–251. [CrossRef]

47. Calamita, F.; Satolli, S.; Scisciani, V.; Esestime, P.; Pace, P. Contrasting styles of fault reactivation in curved orogenic belts: Examples from the Central Apennines (Italy). *Geol. Soc. Am. Bull.* **2011**, *123*, 1097–1111. [CrossRef]

48. Bigi, S.; Milli, S.; Corrado, S.; Casero, P.; Aldega, L.; Botti, F.; Moscatelli, M.; Stanzione, O.; Falcini, F.; Marini, M.; et al. Stratigraphy, structural setting and burial history of the Messinian Laga basin in the context of Apennine foreland basin system. *J. Mediterr. Earth Sci.* **2009**, *1*, 61–84.

49. Marini, M.; Milli, S.; Ravnås, R.; Moscatelli, M. A comparative study of confined vs. semi-confined turbidite lobes from the Lower Messinian Laga Basin (Central Apennines, Italy): Implications for assessment of reservoir architecture. *Mar. Pet. Geol.* **2015**, *63*, 142–165. [CrossRef]

50. Barbieri, M.; Boschetti, T.; Petitta, M.; Tallini, M. Stable isotope (2H, 18O and 87Sr/86Sr) and hydrochemistry monitoring for groundwater hydrodynamics analysis in a karst aquifer (Gran Sasso, Central Italy). *Appl. Geochem.* **2005**, *20*, 2063–2081. [CrossRef]

51. Celico, P.; Fabbrocino, S.; Petitta, M.; Tallini, M. Hydrogeological impact of the Gran Sasso motor-way tunnels (Central Italy). *G. Geol. Appl.* **2005**, *1*, 157–165.

52. De Luca, G.; Di Carlo, G.; Tallini, M. Hydraulic pressure variations of groundwater in the Gran Sasso underground laboratory during Amatrice earthquake of August 24th, 2016. *Ann. Geophys.* **2016**, *59*, AG-7200.

53. De Luca, G.; Di Carlo, G.; Tallini, M. A record of changes in the Gran Sasso groundwater before, during and after the 2016 Amatrice earthquake, central Italy. *Sci. Rep.* **2018**, *8*, 15982. [CrossRef]

54. Petitta, M.; Ranalli, D.; Tallini, M. Schema Idrogeologico del Massiccio del Gran Sasso Centrale (Italia Centrale). *Bollet Soc. Geol. It.* **2002**, *121*.

55. Piacentini, T.; Buccolini, M.; Miccadei, E. The Terminillo, Gran Sasso and Majella Mountains: The 'Old Guardians' of the Tyrrhenian and Adriatic Seas. In *Landscapes and Landforms of Italy*; Springer: Berlin, Germany, 2017.

56. ISPRA. *Carta Geologica d'Italia alla Scala 1:50,000, Foglio 349 "Gran Sasso d'Italia"*; Servizio Geologico d'Italia and Regione Abruzzo: Rome, Italy, 2010.

57. Civita, M. Schematizzazione idrogeologica delle sorgenti normali e delle relative opere di captazione. *Mem. Not. Ist. Geol. Appl.* **1973**, *12*, 1–24.

58. Cantonati, M.; Segadelli, S.; Ogata, K.; Tran, H.; Sanders, D.; Gerecke, R.; Rott, E.; Filippini, M.; Gargini, A.; Celico, F. A global review on ambient Limestone-Precipitating Springs (LPS): Hydrogeological setting, ecology, and conservation. *Sci. Total Environ.* **2016**, *568*, 624–637.

59. Cantonati, M.; Stevens, L.E.; Segadelli, S.; Springer, A.E.; Goldscheider, N.; Celico, F.; Filippini, M.; Ogata, K.; Gargini, A. Ecohydrogeology: The interdisciplinary convergence needed to improve the study and stewardship of springs and other groundwater-dependent habitats, biota, and ecosystems. *Ecol. Indic.* **2020**, *110*, 105803. [CrossRef]

60. Caine, J.S.; Evans, J.P.; Forster, C.B. Fault zone architecture and permeability structure. *Geology* **1996**, *24*, 1025–1028. [CrossRef]

61. Ferracuti, L.; Marinelli, G.; Rusi, S. Idrogeologia e monitoraggio delle sorgenti carsiche del Tavo (massiccio carbonatico del Gran Sasso) e loro implicazioni nella gestione dell'emergenza torbidità. *G. Geol. Appl.* **2006**, *3*, 47–52.

62. Bellotti, E. Nuclear physics at gran sasso. *Nucl. Phys. News* **1991**, *1*, 18–20. [CrossRef]

63. Di Matteo, L.; Valigi, D.; Cambi, C. Climatic characterization and response of water resources to climate change in limestone areas: Considerations on the importance of geological setting. *J. Hydrol. Eng.* **2013**, *18*, 773–779. [CrossRef]

64. Medici, G.; West, L.J. Review of groundwater flow and contaminant transport modelling approaches for the Sherwood Sandstone aquifer, UK; insights from analogous successions worldwide. *Q. J. Eng. Geol. Hydrogeol.* **2022**, *55*, qjegh2021-176. [CrossRef]

65. Di Curzio, D. Hydrogeochemical and hydrodynamic features affecting redox processes in groundwater. *Ital. J. Groundw.* **2019**, *8*, 3. [CrossRef]

66. Bortone, I.; Santonastaso, G.; Erto, A.; Chianese, S.; Di Nardo, A.; Musmarra, D. An innovative in-situ DRAINage system for advanced groundwater reactive TREATment (in-DRAIN-TREAT). *Chemosphere* **2021**, *270*, 129412. [CrossRef]

67. Dai, C.; Zhang, J.B.; Gao, M.T.; Zhang, Y.; Li, J.; Hu, J. Effects of functional group loss on biochar activated persulfate in-situ remediation of phenol pollution in groundwater and its countermeasures. *J. Environ. Manag.* **2023**, *341*, 118076. [CrossRef]

68. Kurniawan, T.A.; Lo, W.; Liang, X.; Goh, H.H.; Othman, M.H.D.; Chong, K.K.; Chew, K.W. Remediation technologies for contaminated groundwater due to arsenic (As), mercury (Hg), and/or fluoride (F): A critical review and way forward to contribute to carbon neutrality. *Sep. Purif. Technol.* **2023**, *314*, 123474. [CrossRef]

69. Johnston, P.B.; Atkinson, T.; Barker, J.; Odling, N. Constraining the uncertainty in fracture geometry using tracer tests. *Hydrogeol. J.* **2009**, *17*, 527–539. [CrossRef]

70. Bauer, H.; Schröckenfuchs, T.C.; Decker, K. Propriedades hidrogeológicas de zonas de falhas em um aquífero carbonático carstificado (Calcários do Norte dos Alpes, Áustria). *Hydrogeol. J.* **2006**, *24*, 1147–1170. [CrossRef]

71. Dai, L.; Zhao, Y.; Yin, C.; Mao, C.; Zhang, P.; Zhou, F.; Yu, X. Spatial and Temporal Dynamics of Drought and Waterlogging in Karst Mountains in Southwest China. *Sustainability* **2023**, *15*, 5545. [CrossRef]